Colloids and Surfaces B: Biointerfaces 160 (2017) 238–246

Contents lists available at ScienceDirect

Colloids and Surfaces B: Biointerfaces

journal homepage: www.elsevier.com/locate/colsurfb

Full length article

Is there any difference in the biological impact of soluble and insoluble degradation products of iron-containing biomaterials?

Natalia S. Fagali[a,*], Claudia A. Grillo[a], Susana Puntarulo[b,c], Mónica A. Fernández Lorenzo de Mele[a,d,*]

[a] Instituto de Investigaciones Fisicoquímicas Teóricas y Aplicadas (INIFTA), Universidad Nacional de La Plata (UNLP) – CONICET, Departamento de Química, Facultad de Ciencias Exactas (CC 16, Suc.4, 1900). La Plata, Argentina
[b] Universidad de Buenos Aires (UBA), Facultad de Farmacia y Bioquímica, Fisicoquímica. Buenos Aires, Argentina
[c] CONICET – Universidad de Buenos Aires (UBA). Instituto de Bioquímica y Medicina Molecular (IBIMOL). Buenos Aires, Argentina
[d] Universidad Nacional de La Plata (UNLP), Facultad de Ingeniería. La Plata, Buenos Aires, Argentina

ARTICLE INFO

Article history:
Received 5 April 2017
Received in revised form 8 September 2017
Accepted 12 September 2017
Available online 14 September 2017

Keywords:
Biodegradable
Iron
Reactive species
Interface
Biomaterials

ABSTRACT

The interactions that could be built between the biomaterials and tissue- microenvironments are very complex, especially in case of degradable metals that generate a broad variety of degradation products. The interfacial problems are particularly relevant for Fe-based materials that have been proposed for the development of biodegradable implants. The cell metabolism could be affected by the accumulation of insoluble Fe-containing degradation products that has been observed *in vitro* and *in vivo* as a coarse granular brownish material around the implant. However, the relative importance of each Fe-species (soluble and insoluble) on the cellular behavior of the surrounding cells, particularly on the generation of reactive species (RS), is not completely elucidated.

The aim of this study is to evaluate the processes occurring at the Fe-biomaterial/cells interfacial region, and to discriminate the effects of soluble and insoluble corrosion products released by the bulk metal (Fe- microparticles (Fe^0p) or Fe^0 ring) on the adjacent cells, mainly in relation to RS generation.

With this purpose Fe^0p and Fe^0 ring were incubated with fibroblast cells (BALB/c 3T3 line) for 24 and 48 h periods. Then different techniques were used, such as the dichlorofluorescein diacetate assay ($DCFH_2$-DA) for detection of RS, acridine orange dye for cell viability, total protein content determinations, Prussian Blue staining and TEM observations. To individualize the effects of soluble and insoluble species, independent experiments with Fe^{3+}-salts were performed. Overall data indicate that RS generation by cells exposed to the degradation products of Fe-based biomaterials is more dependent on the presence of insoluble products than on soluble Fe species.

Published by Elsevier B.V.

1. Introduction

Biocompatibility is the basic requirement for all biomaterials. However, the new biomaterials actively participate of the complex processes implicated in tissue regeneration leading to the new concept of bioadaptability [1]. This innovative idea has been suggested to describe the adaptive interactions that could be built between the biomaterial and tissue-microenvironments. Moreover, this concept may provide a new point of view to investigate the fundamental interactions of biomaterials and the biological environment, and to develop new ideas about biomaterials functionalization.

Biodegradable biomaterials have become the focus of scientific interest due to their diverse and significant biomedical applications [2]. They are highly interesting for osteosynthesis and also for coronary and wound closing devices [3], tracheal stents [4] and the treatment of aneurisms [5]. Their advantages include: the reduction of long term risk such as restenosis, associated to permanent implants and the requirement of only one surgical intervention avoiding the need for implant removal. These properties directly impact on the patient comfort and also reduce medical costs. Mg and Fe-based metals have been proposed as bioadsorbable stents.

* Corresponding authors at: Instituto de Investigaciones Fisicoquímicas Teóricas y Aplicadas (INIFTA), Universidad Nacional de La Plata (UNLP) – CONICET, Departamento de Química, Facultad de Ciencias Exactas (CC 16, Suc.4, 1900). La Plata, Argentina
E-mail addresses: nfagali@inifta.unlp.edu.ar (N.S. Fagali), mmele@inifta.unlp.edu.ar (M.A. Fernández Lorenzo de Mele).

http://dx.doi.org/10.1016/j.colsurfb.2017.09.032
0927-7765/Published by Elsevier B.V.

Previous studies have revealed that pure Fe and Fe-based alloys are "safe" degradable implantable materials because they do not seem to be associated with inflammation, neointimal proliferation or thrombotic events [6], Fe overload or toxicity effect on the main organs [7], embolization or thrombosis [8], local toxicity or abnormal clinical observations [2]. But, spite of many of these reports demonstrated the accumulation of insoluble degradation products as a coarse granular brownish material around the implant [6–10], there are no references about the danger of the presence of those products. Nevertheless, Pierson *et al.* [11] showed that encapsulation of Fe wires within the arterial wall was conducive to corrosion, whereas wires implanted into the arterial lumen in contact with flowing arterial blood experienced minimal corrosion. Corrosion products from the Fe wire were accumulated over 9 months and retained as voluminous flakes that threatened the integrity of the arterial wall. Moreover, histological sections obtained from other studies showed significant amounts of Fe ions that were transported far away from the implant surface [2].

Another example of promissory applications of Fe-containing materials is the use of magnetic Fe-oxide nanoparticles (IONPs) as very efficient negative magnetic resonance imaging contrast agents and for magnetofection, that uses magnetic field to concentrate particles containing nucleic acids into the target cells. There is a wide variety of IONPs with different size, shape, functional group and surface coating that give them specific physical-chemical properties. However, it was demonstrated that uncoated Fe_3O_4 and Fe_2O_3 NPs can cause dissimilar levels of oxidative DNA lesions in lung epithelial cells [12,13]. Additionally, cell death and reactive oxygen species (ROS) production were found after exposure of endothelial cells to Fe_2O_3 NPs [13], while Fe_3O_4 NPs have been associated with better biocompatibility [14,15]. Interestingly, it has been reported that, while Fe_2O_3 particles are insoluble in the extracellular medium, dissolution of particles do occur within the cells, being greater for the smaller microparticles [16]. Measurements of Fe in the culture medium and cells lysate showed that more than 70% of the Fe remained within macrophage cells, probably associated to Fe-binding proteins, whereas only 30% was released out to the cells into the extracellular medium [16].

Previous considerations showed that different type of products are formed and released from the several types of degradable Fe-containing biomaterials. These products may be incorporated into the cells and probably change their physical chemical characteristics (size, solubility, protein-association, etc). Thus, the processes occurring at the interface are complex and the importance of each Fe-species (soluble and insoluble) on the cellular behavior of the surrounding cells, particularly on the generation of RS, is not completely elucidated. The aim of this study is to evaluate the events occurring at the Fe-biomaterial/cells interfacial region, and to differentiate the effects of soluble and insoluble corrosion products released by the metal (Fe-microparticles (Fe^0p) or bulk Fe (Fe^0 ring)) on the adjacent cells, mainly in relation to RS generation.

2. Materials and methods

2.1. Materials

Rings of pure bulk Fe^0 were made from a wire (Specpure 99.9%, thickness = 0.5 mm). The average diameter and weight of the rings were 3.3 mm and 12 mg. Fe^0p were purchased from Riedel de Häen (average particle size ≈150 μm). 2,7- dichlorofluorescein diacetate ($DCFH_2$-DA), $FeCl_3{\cdot}6H_2O$, Acridine Orange dye (AO), Coomassie Brilliant Blue G-250, thioglycolic acid, Chelex 100 sodium, bathophenanthroline disulfonic acid disodium salt hydrate form, potassium ferrocyanide, hydrochloric acid and safranine were purchased from Sigma Aldrich (St. Louis, MO, USA).

2.2. Cells and culture conditions

Fibroblast cells (BALB/c 3T3 line) were kindly granted by Dr. Magdalena Gherardi (Instituto de Investigaciones Biomédicas en Retrovirus y SIDA (INBIRS), Facultad de Medicina, Universidad de Buenos Aires). Fibroblast cells were grown as monolayers in T-25 flasks with DMEM culture medium (CM) (GIBCO- BRL, Los Angeles, USA) supplemented with 10% inactivated fetal calf serum (FCS) (Natocor, Villa Carlos Paz, Córdoba, Argentina), 50 IU/mL penicillin and 50 μg/mL streptomycin sulfate (complete culture medium, CCM) in a humidified incubator at 37 °C and 5% CO_2 atmosphere. Viable cells were counted in a Neubauer haemocytometer by the exclusion Trypan Blue (Sigma, St. Louis, MO, USA) method.

2.3. Incubation with Fe^0 ring, Fe^0 microparticles and Fe^{3+} salt

Fibroblast cells were seeded at a density of 1.5×10^5 cells/well in a 6 wells plate for 24 h. Then, the cells were incubated with Fe^0 rings or Fe^0p for 24 and 48 h and Fe^{3+} salt for 24 h. The Fe^0p were suspended in CCM at a concentration in the 0.25-2.00 mg/mL range and were thoroughly mixed by vortex. To obtain the maximum concentration of Fe^{3+} salt, the appropriated amount of $FeCl_3{\cdot}6H_2O$ was added to CCM and dilution was employed as required. A volume of 3 mL of each mixture was dispensed in each well.

2.4. Assay for RS generation

After treatments, Fe^0 rings were removed with a magnet. These cells, like those treated with Fe^0p or Fe^{3+} salt, were washed with phosphate buffer solution (PBS) twice. The fibroblasts were loaded with 0.5 μM $DCFH_2$-DA [17] in CM for 15 min in darkness. The dye solution was removed, and the cells were washed with PBS twice. The fluorescent compound DCF, generated by radical-dependent oxidation of the probe was measured using an epifluorescence microscope Olympus BX51, equipped with a 460–490 nm excitation filter (Olympus, Tokyo, Japan) connected to an Olympus DP73 (Olympus, Tokyo, Japan) digital color camera. The photographs were taken with an objective of 10X. Images were recorded with the cellSens Software (Olympus, Tokyo, Japan). Analysis of images was done with the free software ImageJ and the Integrated Fluorescence was used as parameter to calculate% Fluorescence relative to control (cells without Fe^0 ring or Fe^0p). Three independent experiments were done and fifteen pictures were taken in each zone (in the case of Fe^0 ring) or in each experiment (in the case of Fe^0p).

2.5. Prussian blue staining

To detect the presence of Fe within the cells Prussian Blue staining was employed. After the incubation, Fe° rings were removed from the cell culture with a magnet. The cells were washed with PBS twice and then were fixed with methanol, washed with distillated water, incubated for 20 min with 5% potassium ferrocyanide in 0.2 N hydrochloric acid, washed with distillated water again and finally counterstained with 0.1% safranine [18,19].

2.6. Quantification of cell viability (Acridine orange dye, AO)

Treatments with Fe^0 rings or Fe^0p were followed by washing with PBS twice. Adherent cells were stained with AO dye (Sigma, St. Louis, MO, USA) and immediately examined by fluorescence microscopy equipped with appropriate filter sets, connected to a digital color camera (Olympus, Tokyo, Japan). The photographs were taken with an objective of 10X. Images were recorded with the cellSens Software (Olympus, Tokyo, Japan) and were analyzed with the free software ImageJ. The percentage (%) of fluorescent

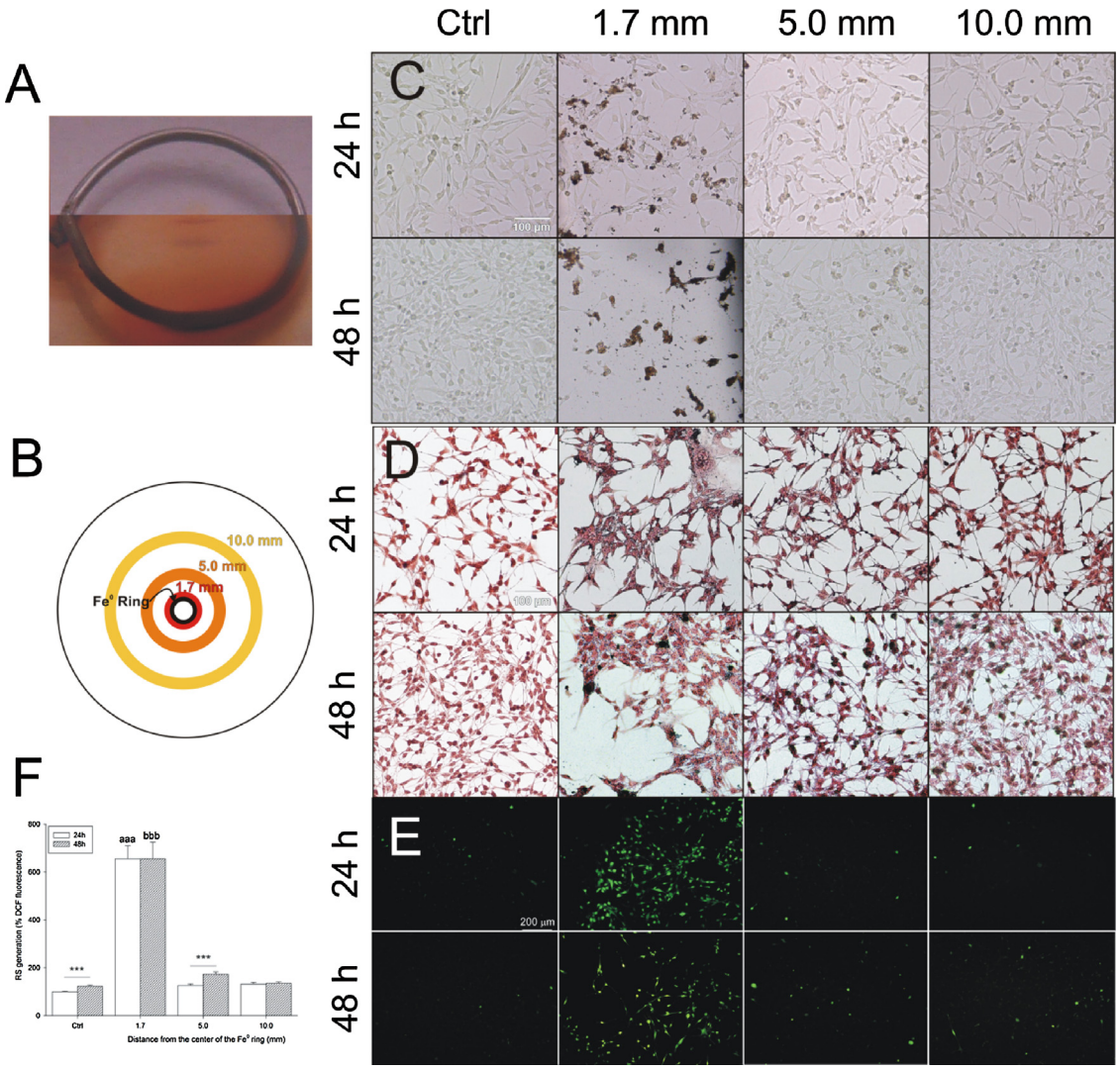

Fig. 1. A) Comparative pictures of Fe^0 ring before (top) and after 7 days of corrosion (bottom) in CCM. **B)** Scheme of the zones around the Fe^0 ring in the culture plate where the pictures were taken (1.7 mm, 5.0 mm and 10 mm): **C)** microphotographs under light microscopy (10X), **D)** Prussian blue staining (10X) and **E)** epifluorescence images (10X) of fibroblast cells loaded with $DCFH_2$-DA. **F)** RS generation expressed as percentage of DCF fluorescence referred to control 24 h (For interpretation of the references to colour in this figure legend, the reader is referred to the web version of this article.)

covered area relative to control was used as parameter of analysis. Three independent experiments were performed and fifteen pictures were taken in each zone (at different distances from the center of the Fe^0 ring) or in each experiment (in the case of Fe^0p).

2.7. TEM observations

For this assay 2×10^4 cells/well (96 well plate) were grown at 37 °C in 5% CO_2 humid atmosphere in CCM for 24 h. This medium was then replaced by fresh CCM and a Fe^0 ring/well (5 wells). After treatments, the CCM was removed and cells were washed with PBS. Monolayers were fixed with 2% glutaraldehyde in phosphate buffer 0.2 M for 2 h at 4 °C. After fixation in 1% OsO_4, samples were embedded in epoxy resin (LX 112, Ladd) and ultrathin sections (60 nm) were obtained by Ultramicrotomy (Leica EM UC7). To enhance contrast, these sections were stained with uranyl acetate solution in alcoholic solution and lead citrate and placed on 150 mesh grids. The cells were examined by TEM (JEOL JEM 1200 EX II). The photographs were obtained with a Erlangshen CCD camera (Model 785 ES1000W Gatan) (Servicio Central de Microscopía Electrónica, Facultad de Ciencias Veterinarias, UNLP).

2.8. Quantification of total proteins

Total protein content was measured following Bradford method [20]. After treatments the cells were washed with PBS twice. A volume of 500 µL of lysis buffer (0.1% Triton in 25 mM Tris-HCl buffer pH = 7.4) was added. The cells were detached with a scrapper and transferred to an eppendorf tube. A volume of 500 µL of buffer Tris-HCl was added and the homogenates were maintained in darkness overnight. The homogenates were gently mixed by vortex and centrifuged to 10000 rpm for 15 min. Aliquots of each supernatant were used for total protein measurements. The absorbance of the Coomassie Brilliant Blue G-250–protein complex solution was measured in a Microplate Reader at 595 nm. Bovine serum albumin (BSA) was used as the standard. Each experiment was repeated three times.

2.9. Quantification of soluble Fe released to culture media

After treatment periods with Fe^0 ring and Fe^0p, the CCM were transferred to 15 mL centrifuge tubes and were centrifuged at 2000 rpm for 15 min to separate insoluble products. An aliquot of 300 µL of supernatant was mixed with equal volume of

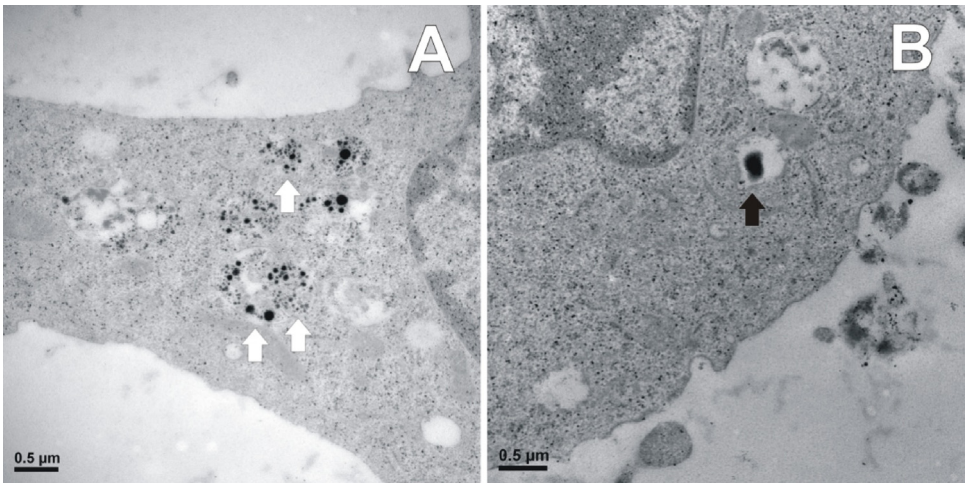

Fig. 2. Transmission electron microscopy photograph (30000X) of fibroblast cells in close contact with Fe^0 ring showing **A)** spherical electron-dense Fe-deposits (ferritin and/or hemosiderin, see white arrows) and **B)** electron-dense fragments of insoluble degradation products (see black arrow).

Table 1
Total protein content corresponding to the attached cells incubated with a Fe^0 ring during 24 and 48 h and **average soluble Fe released** by Fe^0 ring to culture medium (3 mL/well). The RS production is indicated when was present.

	Total protein content (mg)		Soluble Fe release (μg)	
	24 h	48 h	24 h	48 h
Control	0.29 ± 0.02	0.40 ± 0.01 (**)	1.5 ± 0.4	1.5 ± 1.0
Fe^0 ring	0.26 ± 0.01	0.37 ± 0.03 (***)	24 ± 1 (aaa) RS (near the ring)	32 ± 1 (bbb, ***) RS (near the ring)

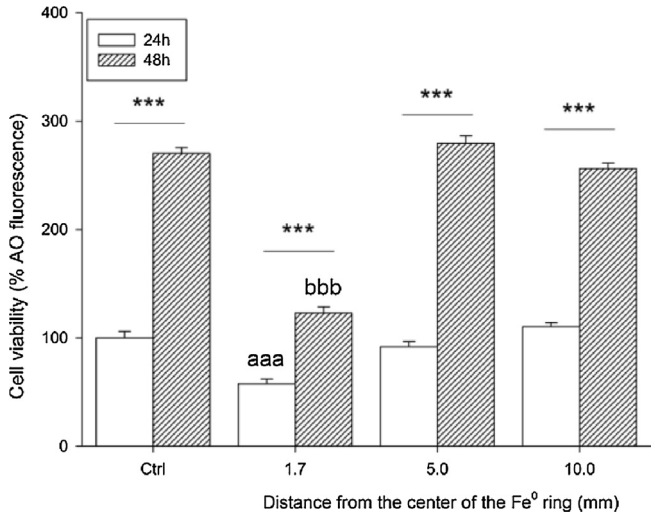

Fig. 3. Cell viability assessed as percentage of AO fluorescence referred to control 24 h of fibroblast cells after incubation for 24 and 48 h with Fe^0 ring.

$HClO_4$:HNO_3 1:1 to disaggregate organic matter. Aliquots of these solutions were mixed with 8% thioglycolic acid, acetate buffer pH 6.0 and 4 mM bathophenanthroline [21]. The absorbance at λ = 535 nm was measured using a Shimadzu UV-1800 spectrophotometer and the Fe concentration was calculated by comparing with standards solutions of Fe^{3+}. All solutions were prepared with MilliQ water treated with Chelex 100 resin to remove contaminating metals. Each experiment was repeated at least three times.

2.10. Statistical analysis

In the figures and tables, results are expressed as $\bar{x} \pm SEM$

Statistical differences were analyzed using ANOVA plus Multiple Range Test of Bonferroni. The statistical significance of differences between means in a pair was indicated by asterisks; differences vs. Control 24 h were indicated with letters "a" and differences vs. Control 48 h were indicated with letters "b" (** $p < 0.01$, ***, aaa and bbb: $p < 0.001$).

3. Results

3.1. Bulk Fe^0 ring

3.1.1. Light microscopy observations, prussian blue staining and RS generation

In Fig. 1A, the insoluble degradation products can be seen as red brownish precipitates near the Fe^0 ring. Fig. 1B shows a scheme of the culture plate with the different zones around the Fe^0 ring where the pictures were taken. The period of incubation in CCM was 7 days to show clearly the accumulation of precipitates.

In the light microscopy images (Fig. 1C), scarce cells with normal morphology and several brownish rounded dead cells in the zone closest to the ring (1.7 mm) can be observed. The particular color of these cells is due to a high intracellular Fe content. It is noteworthy that this observation was done directly, i.e.: without washing steps or culture medium discard. In more distant regions (5.0 and 10.0 mm) the number of cells and morphology are similar to those of control cells.

After Prussian Blue staining (Fig. 1D), intracytoplasmic inclusions were visualized under light microscope as bluestained vesicles in the cells placed in the zone closest to the ring (1.7 mm). The brownish colored cells observed in Fig. 1C, were not present in Fig. 1D because the Prussian Blue technique includes several washing steps which could lead to cell loss. Nevertheless, in this zone the attached cells presented blue granules indicating a high level of stored Fe. These granules were scarce in cells located far from

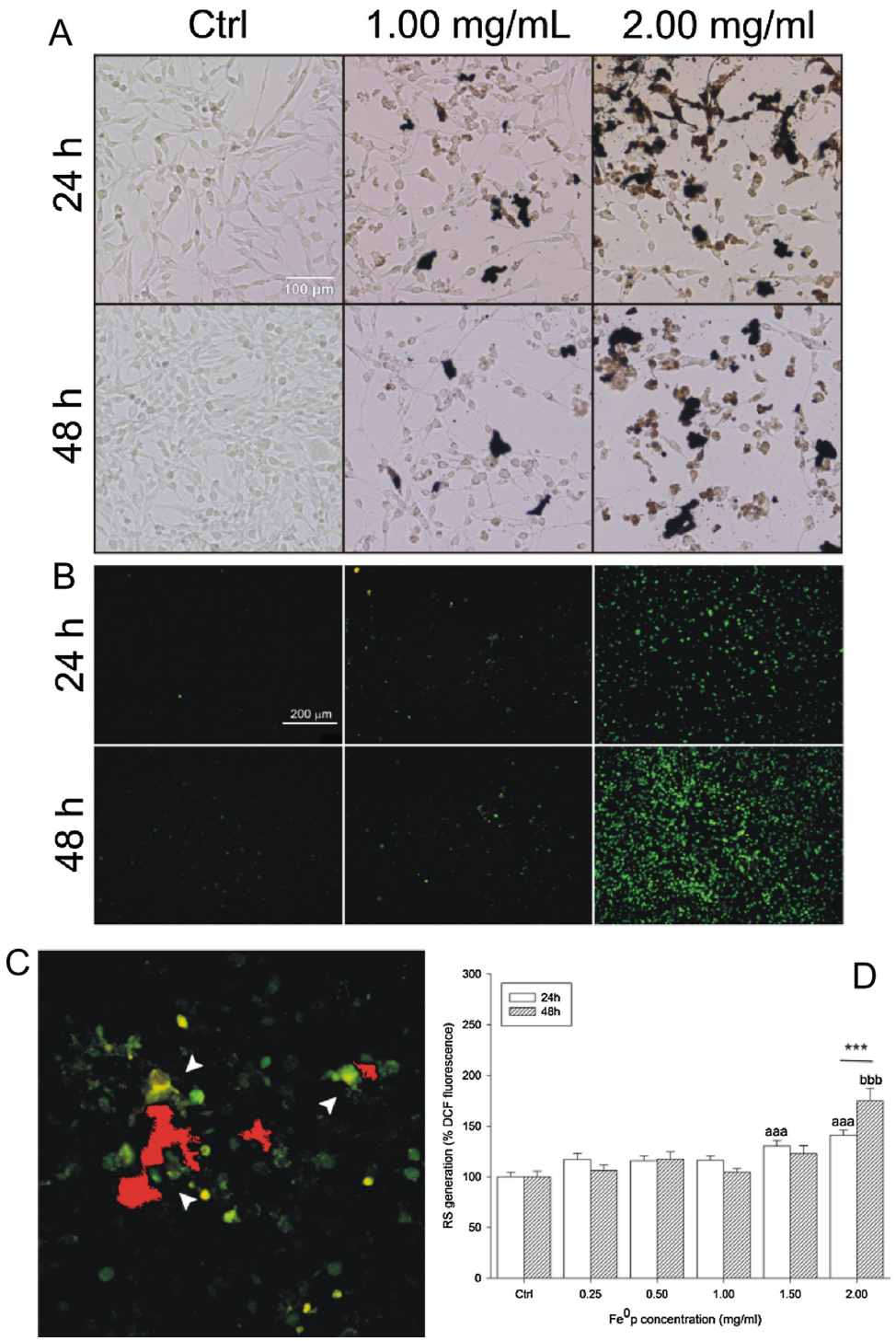

Fig. 4. A) Microphotographs under light microscopy (10X) and **B)** epifluorescence images of fibroblast cells loaded with $DCFH_2$-DA after treatments for 24 and 48 h with 1.00 and 2.00 mg/mL Fe^0p. **C)** Detail of fibroblast cells incubated with 2.00 mg/mL for 48 h. White arrowheads point out the highly fluorescent cells close to Fe^0p highlighted in red. **D)** RS generation expressed as percentage of DCF fluorescence of fibroblast cells exposed to Fe^0p in the 0.25-2.00 mg/mL concentrations range, referred to control 24 h.

the ring. In those areas, the staining was similar to that of control cells.

The RS generation at different distances from the center of the ring is depicted in Fig. 1E and F. A significant increase of RS production in the zone closest to the Fe^0 ring (1.7 mm) compared to control can be seen. The maximum production of RS in this zone was detected after 24 h of incubation and it was maintained after 48 h. In the further zones there are no significant differences with their respective control.

3.1.2. *TEM observations*

TEM observations (Fig. 2) of cells in close contact with Fe^0 ring, revealed two different intracytoplasmatic inclusions distributed in polydispersed vesicles: Spherical electron-dense deposits (Fig. 2A) presumably corresponding to insoluble ferritin or hemosiderin, and electron-dense fragments (Fig. 2B) of insoluble degradation products. Both inclusion types are located in organelles such as phagosomes which indicate that the cells were able to incorporate the fragments of insoluble degradation products by phagocytosis.

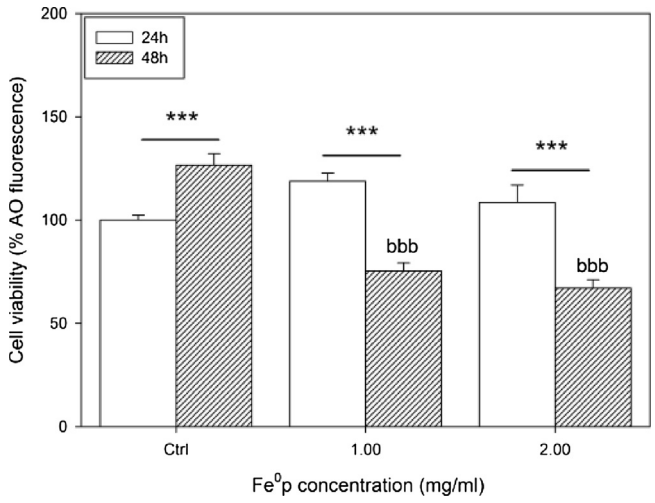

Fig. 5. Cell viability assessed as percentage of AO fluorescence of fibroblast cells after 24 and 48 h incubation time with 1.00 and 2.00 mg/mL Fe^0p, referred to control 24 h.

3.1.3. Cell viability

During the 24 h incubation period a significant decrease in cell viability was noticed (Fig. 3) in the zone nearest to the Fe^0 ring (1.7 mm), while in more distant areas (5.0 and 10.0 mm) the cell survival was not affected. After 48 h, the cell viability in the nearest zone is lower than that of the control 48 h, while in the more distant regions there were no significant differences.

3.1.4. Total protein content

Table 1 shows that the presence of the Fe^0 ring did not significantly affect the total mass of cells represented as total protein, although an increasing local RS and a decreasing cell viability were detected near the Fe^0 ring.

3.1.5. Soluble Fe released to culture medium

Table 1 also shows a significant increase in soluble Fe released to culture medium from the Fe^0 ring from 24 to 48 h of incubation period. It should be emphasized that each value corresponds to the average amount of soluble Fe accumulated in the whole Petri dish during the corresponding period. The data presented in this table point out the presence of RS in cells located together with insoluble degradation products.

3.2. Fe^0p

3.2.1. Light microscopy observations and RS generation

In light microscopy images (Fig. 4A), either cells with normal morphology or scarce brownish rounded dead cells were observed in presence of 1.00 mg/mL Fe^0p after 24 h of incubation. Longer periods of incubation or higher concentration of Fe^0p provoked higher cell damage and cell death. Data in Fig. 4B shows the increase of RS generation in cells exposed to 2.00 mg/mL after 24 and 48 h of incubation, as compared to control cells. Fig. 4C showed a detail of highly fluorescent cells in direct contact with Fe^0p after 24 h of incubation (2.00 mg/mL). The cells produced an enhancement in the RS generation relative to control after 24 h of incubation with 1.50 and 2.00 mg/mL Fe^0p, while after 48 h a significant raise of RS can be observed only at the 2.00 mg/mL (Fig. 4D).

3.2.2. Cell viability

The cell viability after 24 h of incubation with 1.00 and 2.00 mg/mL Fe^0p did not show any significant difference relative to control 24 h (Fig. 5) although RS generation was observed when the cells were exposed to 2.00 mg/mL Fe^0p (Fig. 4B and D). After 48 h of treatment with 1.00 mg/mL Fe^0p the cell viability decreased significantly, in spite of that at this concentration, RS generation was not detected. For the highest concentration analyzed (2.00 mg/mL), the cell viability was also reduced in agreement with the highest RS generation under these conditions.

3.2.3. Total protein content

The total content of protein was assayed as an indicator of the total mass of cells. Data in Table 2 show that the presence of the different concentrations of Fe^0p does not affect the total number of cells despite there are differences in viability and RS production.

3.2.4. Soluble Fe released to culture medium

The level of total soluble Fe released to the culture medium from different concentrations of Fe^0p is shown in Table 2. A proportional increase of released Fe regarding to Fe^0p concentration and time of exposure is observed.

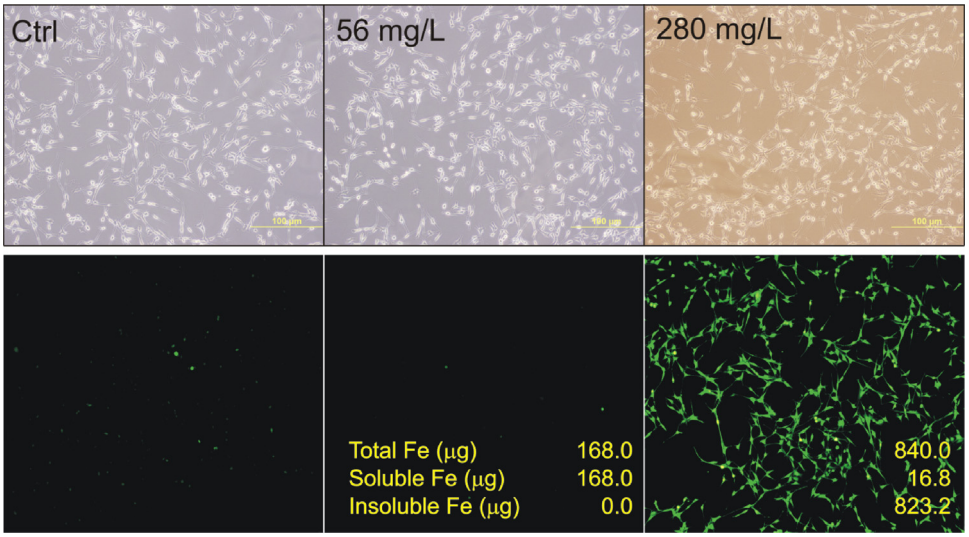

Fig. 6. Light microscopy images (top panel) and epifluorescence images (bottom panel) of fibroblast cells loaded with $DCFH_2$-DA after 24 h treatments with 56 and 280 mg/L of $FeCl_3.6H_2O$. Amounts of total Fe in the culture plate, and soluble and insoluble species formed in each solution are indicated in each figure.

Table 2
Total protein content corresponding to the attached cells exposed to Fe^0p in the 0.00-2.00 mg/mL concentrations range for 24 and 48 h and **average soluble Fe released** from Fe^0p to culture medium (3 mL/well).

Added Fe^0p (mg/ml)	Total protein content (mg)		Soluble Fe release (μg)	
	24h	48h	24h	48h
Control	0.23 ± 0.02	0.40 ± 0.01 (***)	1.3 ± 0.3	1.1 ± 0.3
0.25	0.25 ± 0.02	0.45 ± 0.02 (***)	1.9 ± 0.6	2.5 ± 0.7
0.50	0.24 ± 0.03	0.43 ± 0.04 (***)	3.4 ± 0.5	8.2 ± 0.6
1.00	0.26 ± 0.02	0.43 ± 0.02 (***)	18 ± 2	30 ± 4 (bbb)
1.50	0.26 ± 0.02	0.38 ± 0.01 (***)	22 ± 4	40 ± 4 (bbb)
2.00	0.25 ± 0.02	0.38 ± 0.02 (***)	45 ± 8 (aaa)	86 ± 11(bbb,***)

3.3. Fe^{3+} salt

3.3.1. Light microscopy observations and RS generation

Fig. 6 (top panel) shows microphotographs of cells exposed to two different concentrations of Fe^{3+} salt. The cell morphology is conserved in both cases but the cell number diminished slightly at 280 mg/mL. At 56 mg/L, all the added salt is found in a soluble form while at 280 mg/L a great volume of precipitate is produced, leaving a low concentration of soluble Fe. The precipitate is the reason why the background has a brownish tinge. In this figure, a high production of RS (Fig. 6, bottom panel) can be seen when precipitates are present.

4. Discussion

4.1. About the experimental design

The impact in the human body of metallic biomaterials is often simulated using salts (within the solubility range) with a uniform concentration all through the wells. Moreover, the largest body of evidence found in the literature describes the effect of metal ions [22–25], but there is little information about the accumulation of soluble and insoluble products in the surrounding tissues and their effects. Our experimental set up is very different from those ones because includes a bulk metal as a source of ions and degradation products. The experimental design was intended to answer the following question: Which is/are the responsible form of Fe leading to RS generation in case of Fe-based biomaterials: the insoluble products and/or the high concentration of ions around the metal?

4.2. Bulk Fe^0 ring

The measured concentrations of released soluble Fe are indeed average values (Table 1) obtained by mixing the whole liquid volume of the well. But actually the concentration is not uniform within the plate since there are concentration gradients in the region between Fe source and the well border. The diffusion of ions in the biological media follows a complex relationship derived from the Fickís 2nd law equation [26] that indicates how the concentration is a function of the distance from the ions source increasing with the exposure time. In this way, the concentration of each place increases with time and after 48 h of incubation, all the cells (either near or far from the ring) are exposed to high levels of soluble Fe. Surprisingly, after this long period only the cells in the zone nearest to the ring showed a decrease in viability and RS generation (1E and 3).

Analyzing the complex relationship between RS (and cell viability) *vs.* released soluble Fe it is reasonable to hypothesize that high concentration of soluble Fe is not a sufficient condition to induce cell death. Instead, the cell mortality is directly related to the increase of RS production. Thus, RS generation may be linked to the *direct contact* between cells and *insoluble degradation products* formed in the metal surrounding during degradation process. Accordingly, the cell viability and RS generation are dependent on the distance from the ring, even though the total protein content in the culture plate incubated with the Fe^0 ring, did not vary compared to control. This evidence supports the idea that the *in vivo* harmful effects of Fe-biomaterial degradation products are indeed relevant at a local level (the biomaterial/cell interface) although secondary effects are no detected at a "global" or systemic level.

4.3. Fe^0p

Results with Fe^0p are in agreement with those obtained with the Fe^0 ring. In fact, analyzing Fig. 4C, it is possible to note that the cells in direct contact with Fe^0p show a higher level of fluorescence than those more distant. It is noteworthy to remark that when the concentration of Fe^0p is high, both the number of cells in contact with them and the RS level increase. As in the Fe^0 ring case, there are gradients of released soluble Fe from the particles to the medium. But, it may be supposed that, after 48 h of incubation, when 2.00 mg/mL of Fe^0p are distributed over the entire surface of the well, all the cells are exposed to high levels of soluble Fe released by the particles. However, only the cells in direct contact with the Fe^0p expressed RS generation. This observation confirms that the processes occurring close to insoluble degradation products and not the high concentration of soluble species would be responsible of this deleterious effect. This exclusive dependence on insoluble degradation products and RS production is not valid for cell viability in presence of Fe^0p. In fact, a long exposure (48 h) to 1.00 mg/mL of Fe^0p, is enough to affect cell viability even if RS generation is not detected. Then, cell viability in this case seems to be dependent on other factors like the mechanical damage produced by the Fe^0p.

4.4. Comparison of released soluble Fe by Fe^0 ring and Fe^0p

It is also important to take into account that after 48 h of incubation, a Fe^0 ring of 12 mg released an average amount of ≈30 μg (Table 1) of soluble Fe to the medium (3 mL/well); while 6 mg of Fe^0p (half the weight of a ring) released more than twice (≈85 μg, Table 2). Thus, the higher exposed area of the particles turns them more susceptible to corrosion with a higher release of degradation products. Consequently, it is possible to infer that, in clinical situations when the bulk Fe-based biomaterial corrodes, the presence of low concentrations of soluble Fe (without insoluble products formation) can be better handled by the organism. However, if the Fe biomaterial degrades by fragmentation into particles, the release of soluble Fe is higher. Moreover, the particles may travel and reach new tissues and organs and produce alterations at the systemic level.

4.5. Role of soluble and insoluble species

In order to elucidate the particular role of soluble and insoluble species in the generation of RS, more evidence was sought. Independent experiments with Fe^{3+} salt, at concentrations higher (280 mg/L) and lower (56 mg/L) than that of the solubility limit (in culture medium this limit is over 112 mg/L) [21] were studied and the results were compared with those obtained with Fe^0 rings and Fe^0p. Results informed in a previous work [21] revealed that serum compounds (mainly proteins), that are in the culture medium formulation, are closely involved in the solubility and degradation process. In agreement, data in Fig. 6 show that at 56 mg/L of Fe^{3+} salt, all the Fe was in a soluble form, while at 280 mg/L of the metal salt, the concentration of soluble Fe was very low since it was dragged by protein-containing precipitates [27]. In view of these results, it can be noted that the presence of high amounts of soluble Fe (168 μg without precipitates, Fig. 6) did not lead to RS generation while low levels of soluble Fe (≈15–30 μg, Table 1 and Fig. 6) together with precipitates yield to RS production. Importantly, the RS production was detected just in the zones where precipitates were found (Fig. 1A and E). This experimental evidence confirmed the active role of insoluble products in the generation of RS.

On the same line of results, Lin *et al.* [28] found that corrosion particles precipitating during extraction and incubation of nitride Fe stents were significantly toxic to L929 fibroblasts. However, when such precipitation was prevented or minimized, extracts with Fe ion concentration up to 124 mg/L showed no cytotoxicity to L929 fibroblasts. Strikingly, Zhu *et al.* [22] found a significant decrease in metabolic activity of endothelial cells exposed to concentrations of Fe ions higher than 100 mg/L. However, the researchers did not mention the presence of precipitates presumably since such effect is typically neglected. It is noteworthy to mention that in both cases, the solubility limit for protein-containing media (≈112 mg/L) was exceeded. In agreement with present results, a previous work of our group [29] demonstrated that degradation of Mg-based alloys provoked a dramatic decrease in lysosomal activity of CHO-K1 cells while this effect was not observed with filtered extracts (without insoluble corrosion products). Again, insoluble products were responsible of the deleterious effect.

Liu and Wang (2013) [19] investigated DMSA-coated Fe_3O_4 nanoparticles (Fe-NPs) on cell gene expression and concluded that the Fe-NPs might be more detrimental to cell than Fe ion due to its mode of intracellular internalization. Until now, all studies on internalization mechanism of Fe-NPs concluded that NPs entered cells by nonspecific endocytosis [14,16], especially clathrin-mediated endocytosis while Fe ions enter cells by receptor-mediated endocytosis. These authors also suggest that the effects on gene expression are triggered by a high intracellular level of Fe ions coming from the NPs degradation in the lysosome milieu. The gene expression reflects a compensatory response against the rise of intracellular Fe ions. However, they consider that NPs internalization by phagocytosis could not be regulated by the cells. In agreement with these concerns, data presented here demonstrate that cells are able to store Fe (1D and 3A) as ferritin or hemosiderin [30]. On the other hand, TEM microphotographs show that submicron fragments of insoluble Fe products could also be internalized by the cell by phagocytosis (Fig. 3B) without any cellular regulation of this internalization. Subsequently, Fe particles can be degraded in lysosomes, raising the Fe ion concentration and triggering RS production, among other unknown reactions followed by cell death. In our previous work with Fe^{3+} salt, including a range of concentrations that overreach the soluble limit [21], it was demonstrated that cells were able to incorporate the precipitates and generate lipid peroxidation.

Finally, current study also helps to understand that the accumulation of insoluble degradation Fe products in tissues nearby the implant, can originate deleterious reactions at local level, even in absence of systemic damage.

5. Concluding remarks

Assays performed with Fe^0 rings and Fe^0p confirm that the Fe-containing materials degradation in biological environment involves both soluble and insoluble Fe species. However, results demonstrated that cell viability may not be affected by high concentrations of soluble Fe. RS generation and the concomitant cell death are mainly associated to the presence of insoluble degradation products. Taking into account that the role of Fe and RS in cell death are cause of controversy [31], this work is a step forward to the elucidation of this issue.

Acknowledgments

This study was supported by CONICET and grants from the ANPCyT (PICT 2012-1795, PICT 2015-0232, PICT 2016-1424>) and University of La Plata (11-I221). The authors are very grateful to Dra. Magdalena Gherardi, Dra. Patricia Battistoni, Dr. Ángel Catalá, TB Roxana Peralta and Dra. Susana Jurado for their valuable help.

References

[1] Y. Wang, Bioadaptability: an innovative concept for biomaterials, J. Mater. Sci. Technol. (2016) 1–9, http://dx.doi.org/10.1016/j.jmst.2016.08.002.
[2] T. Kraus, F. Moszner, S. Fischerauer, M. Fiedler, E. Martinelli, J. Eichler, F. Witte, E. Willbold, M. Schinhammer, M. Meischel, P.J. Uggowitzer, J.F. Löffler, A. Weinberg, Biodegradable Fe-based alloys for use in osteosynthesis: outcome of an in vivo study after 52 weeks, Acta Biomater. 10 (2014) 3346–3353, http://dx.doi.org/10.1016/j.actbio.2014.04.007.
[3] A.C. Hänzi, A. Metlar, M. Schinhammer, H. Aguib, T.C. Lüth, J.F. Löffler, P.J. Uggowitzer, Biodegradable wound-closing devices for gastrointestinal interventions: degradation performance of the magnesium tip, Mater. Sci. Eng. C. 31 (2011) 1098–1103, http://dx.doi.org/10.1016/j.msec.2011.03.012.
[4] A.H.C. Ng, N.S.P. Ng, G.H. Zhu, L.H.Y. Lim, S.S. Venkatraman, A fully degradable tracheal stent: in vitro and in vivo characterization of material degradation, J. Biomed. Mater. Res. Part B Appl. Biomater 100 B (2012) 693–699, http://dx.doi.org/10.1002/jbm.b.32501.
[5] K. Wang, S. Yuan, X. Zhang, Q. Liu, Q. Zhong, R. Zhang, P. Lu, J. Li, Biodegradable flow-diverting device for the treatment of intracranial aneurysm: short-term results of a rabbit experiment, Neuroradiology 55 (2013) 621–628, http://dx.doi.org/10.1007/s00234-013-1150-0.
[6] M. Peuster, P. Wohlsein, M. Brügmann, M. Ehlerding, K. Seidler, C. Fink, H. Brauer, A. Fischer, G. Hausdorf, A novel approach to temporary stenting: degradable cardiovascular stents produced from corrodible metal-results 6–18 months after implantation into New Zealand white rabbits, Heart 86 (2001) 563–569, http://dx.doi.org/10.1136/heart.86.5.563.
[7] M. Peuster, C. Hesse, T. Schloo, C. Fink, P. Beerbaum, C. von Schnakenburg, Long-term biocompatibility of a corrodible peripheral iron stent in the porcine descending aorta, Biomaterials 27 (2006) 4955–4962, http://dx.doi.org/10.1016/j.biomaterials.2006.05.029.
[8] R. Waksman, R. Pakala, R. Baffour, R. Seabron, D. Hellinga, F.O. Tio, Short-term effects of biocorrodible iron stents in porcine coronary arteries, J. Interv. Cardiol. 21 (2008) 15–20, http://dx.doi.org/10.1111/j.1540-8183.2007.00319.x.
[9] Q. Feng, D. Zhang, C. Xin, X. Liu, W. Lin, W. Zhang, S. Chen, K. Sun, Characterization and in vivo evaluation of a bio-corrodible nitrided iron stent, J. Mater. Sci. Mater. Med. 24 (2013) 713–724, http://dx.doi.org/10.1007/s10856-012-4823-z.
[10] A. Francis, Y. Yang, S. Virtanen, A.R. Boccaccini, Iron and iron-based alloys for temporary cardiovascular applications, J. Mater. Sci. Mater. Med. 26 (2015) 138, http://dx.doi.org/10.1007/s10856-015-5473-8.
[11] D. Pierson, J. Edick, A. Tauscher, E. Pokorney, P. Bowen, J. Gelbaugh, J. Stinson, H. Getty, C.H. Lee, J. Drelich, J. Goldman, A simplified in vivo approach for evaluating the bioabsorbable behavior of candidate stent materials, J. Biomed. Mater. Res. B. Appl. Biomater. 100 (2012) 58–67, http://dx.doi.org/10.1002/jbm.b.31922.
[12] H.L. Karlsson, J. Gustafsson, P. Cronholm, L. Möller, Size-dependent toxicity of metal oxide particles—A comparison between nano- and micrometer size, Toxicol. Lett. 188 (2009) 112–118, http://dx.doi.org/10.1016/j.toxlet.2009.03.014.

[13] A. Hanini, A. Schmitt, K. Kacem, F. Chau, S. Ammar, J. Gavard, Evaluation of iron oxide nanoparticle biocompatibility, Int. J. Nanomed. 6 (2011) 787–794, http://dx.doi.org/10.2147/IJN.S17574.
[14] Y. Liu, Z. Chen, J. Wang, Systematic evaluation of biocompatibility of magnetic Fe3O4 nanoparticles with six different mammalian cell lines, J. Nanoparticle Res. 13 (2011) 199–212, http://dx.doi.org/10.1007/s11051-010-0019-y.
[15] K. Müller, J.N. Skepper, M. Posfai, R. Trivedi, S. Howarth, C. Corot, E. Lancelot, P.W. Thompson, A.P. Brown, J.H. Gillard, Effect of ultrasmall superparamagnetic iron oxide nanoparticles (Ferumoxtran-10) on human monocyte-macrophages in vitro, Biomaterials 28 (2007) 1629–1642, http://dx.doi.org/10.1016/j.biomaterials.2006.12.003.
[16] I. Beck-Speier, W.G. Kreyling, K.L. Maier, N. Dayal, M.C. Schladweiler, P. Mayer, M. Semmler-Behnke, U.P. Kodavanti, Soluble iron modulates iron oxide particle-induced inflammatory responses via prostaglandin E(2)synthesis: in vitro and in vivo studies, Part. Fibre Toxicol. 6 (2009) 34, http://dx.doi.org/10.1186/1743-8977-6-34.
[17] A. Aranda, L. Sequedo, L. Tolosa, G. Quintas, E. Burello, J. Castell, L. Gombau, Dichloro-dihydro-fluorescein diacetate (DCFH-DA) assay: a quantitative method for oxidative stress assessment of nanoparticle-treated cells, Toxicol. Vitro 27 (2013) 954–963, http://dx.doi.org/10.1016/j.tiv.2013.01.016.
[18] H. Parsa, K. Shamsasenjan, A. Movassaghpour, P. Akbarzadeh, B. Amoghli Tabrizi, N. Dehdilani, P. Lotfinegad, F. Soleimanloo, Effect of superparamagnetic iron oxide nanoparticles-Labeling on mouse embryonic stem cells, Cell J. 17 (2015) 221–230, http://dx.doi.org/10.22074/cellj.2016.3719.
[19] Y. Liu, J. Wang, Effects of DMSA-coated Fe3O4 nanoparticles on the transcription of genes related to iron and osmosis homeostasis, Toxicol. Sci. 131 (2013) 521–536, http://dx.doi.org/10.1093/toxsci/kfs300.
[20] M.M. Bradford, A rapid and sensitive method for the quantitation of microgram quantities of protein utilizing the principle of protein-dye binding, Anal. Biochem. 72 (1976) 248–254, http://dx.doi.org/10.1016/0003-2697(76)90527-3.
[21] N.S. Fagali, C.A. Grillo, S. Puntarulo, M.A. Fernández, L. De Mele, Cytotoxicity of corrosion products of degradable Fe-based stents: relevance of pH and insoluble products, Colloids Surf. B Biointerfaces 128 (2015) 480–488, http://dx.doi.org/10.1016/j.colsurfb.2015.02.047.
[22] S. Zhu, N. Huang, L. Xu, Y. Zhang, H. Liu, H. Sun, Y. Leng, Biocompatibility of pure iron: in vitro assessment of degradation kinetics and cytotoxicity on endothelial cells, Mater. Sci. Eng. C. 29 (2009) 1589–1592, http://dx.doi.org/10.1016/j.msec.2008.12.019.
[23] P.P. Mueller, T. May, A. Perz, H. Hauser, M. Peuster, Control of smooth muscle cell proliferation by ferrous iron, Biomaterials 27 (2006) 2193–2200, http://dx.doi.org/10.1016/j.biomaterials.2005.10.042.
[24] M. Moravej, A. Purnama, M. Fiset, J. Couet, D. Mantovani, Electroformed pure iron as a new biomaterial for degradable stents: in vitro degradation and preliminary cell viability studies, Acta Biomater. 6 (2010) 1843–1851, http://dx.doi.org/10.1016/j.actbio.2010.01.008.
[25] B. Liu, Y.F. Zheng, Effects of alloying elements (Mn, Co, Al, W, Sn, B, C and S) on biodegradability and in vitro biocompatibility of pure iron, Acta Biomater. 7 (2011) 1407–1420, http://dx.doi.org/10.1016/j.actbio.2010.11.001.
[26] M.D. Pereda, M. Reigosa, M.A. Fernández Lorenzo, Relationship between radial diffusion of copper ions released from a metal disk and cytotoxic effects. Comparison with results obtained using extracts, Bioelectrochemistry 72 (2008) 94–101, http://dx.doi.org/10.1016/j.bioelechem.2007.11.008.
[27] M. Pivokonsky, J. Safarikova, P. Bubakova, L. Pivokonska, Coagulation of peptides and proteins produced by Microcystis aeruginosa: interaction mechanisms and the effect of Fe-peptide/protein complexes formation, Water Res. 46 (2012) 5583–5590, http://dx.doi.org/10.1016/j.watres.2012.07.040.
[28] W. Lin, G. Zhang, P. Cao, D. Zhang, Y. Zheng, R. Wu, L. Qin, G. Wang, T. Wen, Cytotoxicity and its test methodology for a bioabsorbable nitrided iron stent, J. Biomed. Mater. Res. B Appl. Biomater. (2014) 1–13, http://dx.doi.org/10.1002/jbm.b.33246.
[29] C.A. Grillo, F. Alvarez, M.A. Fernández, L. De Mele, Degradation of bioabsorbable Mg-based alloys: assessment of the effects of insoluble corrosion products and joint effects of alloying components on mammalian cells, Mater. Sci. Eng. C. 58 (2016) 372–380, http://dx.doi.org/10.1016/j.msec.2015.08.043.
[30] C. Quintana, L. Gutiérrez, Could a dysfunction of ferritin be a determinant factor in the aetiology of some neurodegenerative diseases? Biochim. Biophys. Acta – Gen. Subj. 2010 (1800) 770–782, http://dx.doi.org/10.1016/j.bbagen.2010.04.012.
[31] S.J. Dixon, B.R. Stockwell, The role of iron and reactive oxygen species in cell death, Nat. Chem. Biol. 10 (2013) 9–17, http://dx.doi.org/10.1038/nchembio.1416.